Modified long-range surface plasmon polariton modes for laser nanoresonators

Kazuhiro Ikeda,[1,a)] Yeshaiahu Fainman,[2] K. Alan Shore,[3] and Hitoshi Kawaguchi[1]
[1]*Graduate School of Materials Science, Nara Institute of Science and Technology, 8916-5 Takayama, Ikoma, Nara 630-0192, Japan*
[2]*Department of Electrical and Computer Engineering, University of California, San Diego, 9500 Gilman Drive, La Jolla, California 92093-0407, USA*
[3]*School of Electronic Engineering, Bangor University, Bangor, LL57 1 UT, Wales, United Kingdom*

(Received 12 May 2011; accepted 11 August 2011; published online 19 September 2011)

We investigate a modification of long-range surface plasmon polariton modes supported by thin metal-coated dielectric cylinders for laser nanoresonators. A drawback of the low loss surface modes is the small mode overlap with the core dielectric cylinder that will be intended for the gain region in typical nanolasers. We show that increasing the refractive index of the outermost dielectric cladding improves the poor mode overlap, but still keeps the mode low loss and well confined in a small radius of the cylinder. The high refractive index of the dielectric cladding offers another possibility of a nanolaser structure whose gain region resides in the cladding. © *2011 American Institute of Physics*. [doi:10.1063/1.3638704]

I. INTRODUCTION

A large number of studies of nanolasers with metal claddings have been recently conducted[1–4] where the size of resonators can be smaller than the diffraction limit of light. The mode with the smallest modal cross-sectional area in such metal-clad nanolasers is the lowest-order surface plasmon polariton (SPP) mode localized at the metal-dielectric interface (e.g., TM_{0SP} mode in Ref. 5). These modes however suffer from a significant ohmic loss in the metal, and thus most metal clad nanolasers operating at room temperature utilized the non-SPP TE and HE modes.[1–4] Other interesting modes will be low loss "long-range" SPP modes (e.g., TM_{01} mode in Ref. 5), which have been investigated in thin planar[6–9] and cylindrical[5,10] metal films. In thin metal-coated semiconductor nanocylinders embedded in a lower index dielectric, which may be a useful geometry for nanolasers, a long-range SPP mode is the second-order TM mode altered from the fundamental TM mode in the pure dielectric counterpart without the thin metal shell.[5,10] Although the long-range SPP mode can be supported in smaller cylinders with much smaller attenuation compared to the non-SPP TE and HE modes, the mode overlap with the core semiconductor intended for the current driven gain region is very small,[5] which prohibits efficient amplification. In this article, we investigate a modification of the long-range SPP mode to improve the poor mode overlap with the core semiconductor. In particular, we show that increasing the refractive index of the outermost dielectric cladding improves the poor mode overlap, but still keeps the mode low loss and well confined in a small radius of the cylinder.

II. THEORY

Figure 1 shows the schematic diagram of the structure under investigation. We take the materials and their parameters from Ref. 5. Specifically, the materials for core semiconductor and thin metal shell are assumed to be $In_{0.2}Ga_{0.8}As$ with a refractive index n_1 of 3.6 and gold with a refractive index n_2 of 0.22–j6.71, respectively, where the wavelength is fixed to 1 μm. The wavelength of light used throughout this article is 1 μm. The core radius is defined as r_1 and the metal shell thickness is assumed to be 20 nm. The outermost dielectric is allowed to have different refractive indexes n_3. In this article, we consider an infinitely long cylinder without capping the waveguide ends to analyze the propagation modes.

For eigen-mode analysis of the structure presented in Fig. 1, we use the matrix method[5,11,12] to represent and solve the boundary conditions. Every field component is represented in the form,

$$\psi(r,\theta,z,t) = \psi(r,\theta)e^{j(\beta z-\omega t)}, \tag{1}$$

where ψ can be E_z, E_r, E_θ, H_z, H_r, H_θ; ω is the angular frequency; and β is the propagation constant. Since the transverse field components can be expressed in terms of E_z and H_z using Maxwell's equations, we only need to find solutions for E_z and H_z satisfying the wave equation. The general solutions can be written as

$$E_{zi} = [A_i J_l(k_i r) + B_i Y_l(k_i r)]\cos(l\theta + \varphi_i), \tag{2}$$

$$H_{zi} = [C_i J_l(k_i r) + D_i Y_l(k_i r)]\cos(l\theta + \phi_i), \tag{3}$$

where A_i, B_i, C_i, D_i, φ_i, and ϕ_i are constants, l is the azimuthal number, $i = 1, 2, 3$ represent the regions in the structure that are the core semiconductor, metal shell, and outermost dielectric, respectively, and $k_i = [(\omega/c)^2 n_i^2 - \beta^2]^{1/2}$. The boundary conditions at each interface are that E_z, E_θ, H_z, and H_θ are continuous. Therefore, a 4 x 4 matrix can be found that relates A_i, B_i, C_i, D_i to A_{i+1}, B_{i+1}, C_{i+1}, D_{i+1}, and the final expression representing the multi-interface boundary condition for our structure will be written in a simple form.

a)Electronic mail: kazikeda@ms.naist.jp.

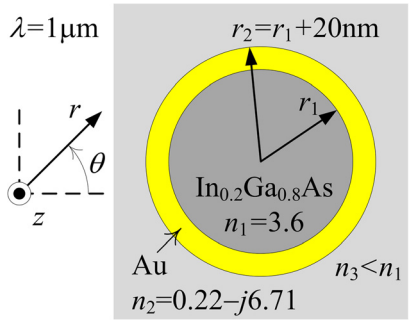

FIG. 1. (Color online) Schematic diagram of a thin metal-coated semiconductor nanocylinder embedded in a lower index dielectric.

$$\begin{pmatrix} A_3 \\ B_3 \\ C_3 \\ D_3 \end{pmatrix} = M \begin{pmatrix} A_1 \\ B_1 \\ C_1 \\ D_1 \end{pmatrix}. \tag{4}$$

The finite field at the center of core and the decaying field in the outermost dielectric impose $B_1 = 0$, $D_1 = 0$, $B_3 = jA_3$, and $D_3 = jC_3$, leading to

$$\begin{pmatrix} M_{11} & -1 & M_{13} & 0 \\ M_{21} & -j & M_{23} & 0 \\ M_{31} & 0 & M_{33} & -1 \\ M_{41} & 0 & M_{43} & -j \end{pmatrix} \begin{pmatrix} A_1 \\ A_3 \\ C_1 \\ C_3 \end{pmatrix} = 0. \tag{5}$$

We then obtain the eigen equation by making the determinant of the matrix in Eq. (5) equal to zero

$$\begin{vmatrix} M_{11} & -1 & M_{13} & 0 \\ M_{21} & -j & M_{23} & 0 \\ M_{31} & 0 & M_{33} & -1 \\ M_{41} & 0 & M_{43} & -j \end{vmatrix} = 0. \tag{6}$$

When we restrict our analysis to the TE or TM mode with $l = 0$, the matrix is block diagonalized and the eigen equation becomes simpler. Finding the mode effective index n_{eff} in the complex plane that satisfies Eq. (6) provides the dispersion and loss or gain characteristics of the propagating modes. In this article, we show results for three low order modes (TE_{01}, TM_{01}, HE_{11}) that are potentially useful for lasing in a small radius of cylinder ($r_1 \sim 200$ nm). However, we exclude the short-range SPP modes (TM_{0SP} and HE_{lSP}) since their propagation losses are way higher than the three modes.[5]

III. MODIFIED LONG-RANGE SPP MODES

A. TE_{01} mode

Although the TE_{01} mode is not a SPP mode, we briefly discuss this mode to compare with the following two long-range SPP modes (TM_{01} and HE_{11}). Figures 2(a), 2(b), and 2(c) show the real and imaginary parts of the calculated n_{eff}, and the Poynting vector confinement factor to the core, respectively, in relation to r_1 for the TE_{01} mode with $n_3 = 1$, 1.45, and 2. The modes with $n_3 = 3$ and 3.5 have the cutoff radius larger than 300 nm and thus are missing in these figures. We observe that the change of n_3 does not affect the effective index much, and only increases the cutoff radius. Figure 3 plots the Poynting vector in z direction with regard to r when $n_3 = 1$, $r_1 = 150$, and 240 nm, indicating the mode confinement to the core. Because of the small imaginary part of effective index (i.e., small attenuation) for r_1 larger than ~300 nm and also the large confinement factor, this mode will be useful for lasing in a large metal-coated cylinder as already pointed out.[3,5,12]

B. TM_{01} mode

Figures 4(a), 4(b), and 4(c) show the real and imaginary parts of the calculated n_{eff}, and the Poynting vector confinement factor to the core, respectively, in relation to r_1 for the TM_{01} mode with $n_3 = 1$ to 3.5. We see from Fig. 4(a) that the real part of n_{eff} ranges between n_1 and n_3 and also that the cutoff radius slightly increases up to 180 nm with increasing n_3. This is similar to the behavior of pure dielectric waveguide modes in which, however, the cutoff radius increases more drastically. Our calculation shows that the

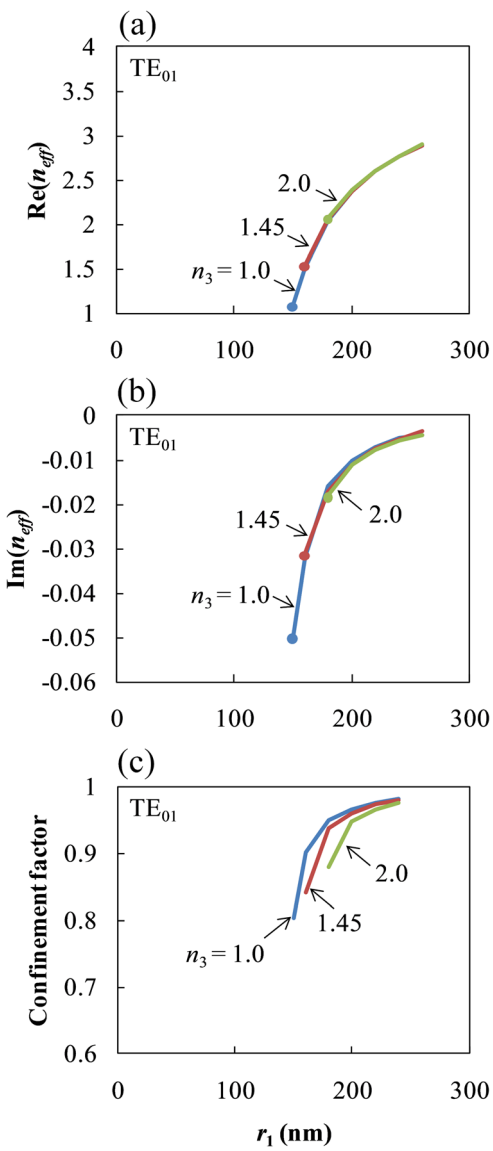

FIG. 2. (Color online) (a) Real and (b) imaginary parts of the calculated n_{eff} and (c) Poynting vector confinement factor, in relation to r_1 for the TE_{01} mode with $n_3 = 1$ to 2.

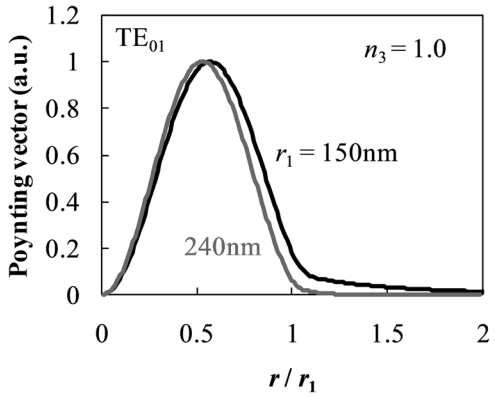

FIG. 3. Poynting vector in z direction vs r for the TE_{01} mode when $n_3 = 1$, $r_1 = 150$ and 240 nm.

cutoff radius for the pure dielectric cylinder with the cladding index of 3.5 reaches 500 nm, which indicates the tight confinement effect of the metal shell. Another observation from Figs. 4(a)–4(c) is that the real and imaginary parts of n_{eff} and the confinement factor increase for $n_3 = 1 \sim 2$ when r_1 becomes larger than ~200 nm. This is because the mode residing mostly in the outermost dielectric for r_1 smaller than 200 nm changes to that mostly in the core semiconductor whose mode profile looks similar to that in the pure dielectric counterpart.[5] Figure 5(a) shows the Poynting vector in z direction with regard to r when $n_3 = 1$, $r_1 = 100$ and 220 nm. Therefore, in the case of air cladding, although the mode with r_1 smaller than 200 nm has a very small loss, the mode overlap with gain is tiny and thus the long-range SPP mode is not useful for gain-assisted propagation.

On the other hand, for $n_3 > 3$, which we introduced in this article, the above change in the nature of the mode around $r_1 = 200$ nm does not occur. Surprisingly, the mode overlap is fairly large as shown in Fig. 4(c) while the modal loss is still low as in Fig. 4(b). Figures 5(b) and 5(c) depict the Poynting vector and field distributions for $n_3 = 3.5$, $r_1 = 180$ nm to clarify the power confinement to the core and the similarity of the field directions (i.e., radial electric fields) to the fundamental TM mode in pure dielectric cylindrical waveguides. An intuitive understanding for the higher mode confinement with a high index cladding may be analogous to the opposite case for the mode distribution in the high index contrast waveguides.[13,14] In other words, the electric fields normal to the core-clad interface are discontinuous at the interface and larger in the low index cladding, in order to satisfy the boundary condition. Since the discontinuity becomes smaller as the index contrast becomes smaller, a higher mode confinement in the core is achieved with a low index contrast as seen in our case. Although there is a thin metal shell between the core and cladding in our structure, the above understanding will still hold since the fields at both sides of the metal shell are well coupled. The advantage of having the metal shell is again to keep the cutoff radius small even when the index contrast is made small.

C. HE_{11} mode

Figures 6(a), 6(b), and 6(c) show the real and imaginary parts of the calculated n_{eff}, and the Poynting vector confinement factor to the core, respectively, in relation to r_1 for the HE_{11} mode with $n_3 = 1$ to 3.5. Figure 7(a) shows the Poynting vector in z direction at an azimuth of $\theta = 0$ deg with regard to r when $n_3 = 1$, $r_1 = 120$ and 180 nm. We observe from these figures the similar behavior to that seen in the TM_{01} mode, in particular, the change from the less lossy mode residing in the outermost dielectric to the highly lossy mode residing in the core semiconductor as r_1 increases when n_1 is small. Therefore, this long-range SPP mode with r_1 smaller than ~150 nm is again not useful for gain-assisted propagation in the case of low index cladding since the mode overlap with gain is tiny. However, for $n_3 > 3$, the change does not occur and the modal loss is kept low while the confinement factor is fairly large. Figures 7(b), 7(c), and 7(d) depict the Poynting vector at $\theta = 0$ deg, field distributions at $\theta = 0$ and 90 deg, respectively, for $n_3 = 3.5$, $r_1 = 180$ nm to clarify the power confinement to the core and the field directions. Thus, introducing the high index outermost cladding

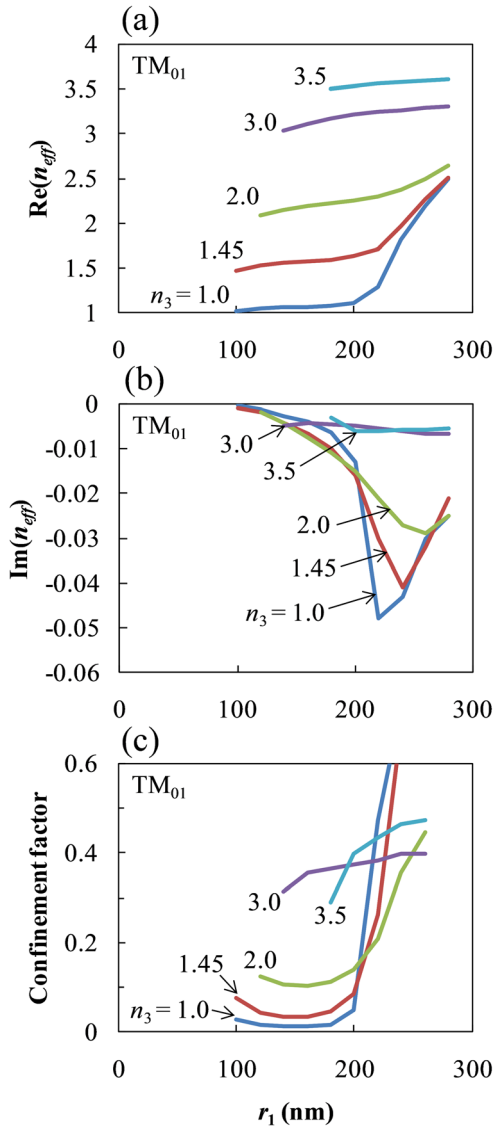

FIG. 4. (Color online) (a) Real and (b) imaginary parts of the calculated n_{eff} and (c) Poynting vector confinement factor, in relation to r_1 for the TM_{01} mode with $n_3 = 1$ to 3.5.

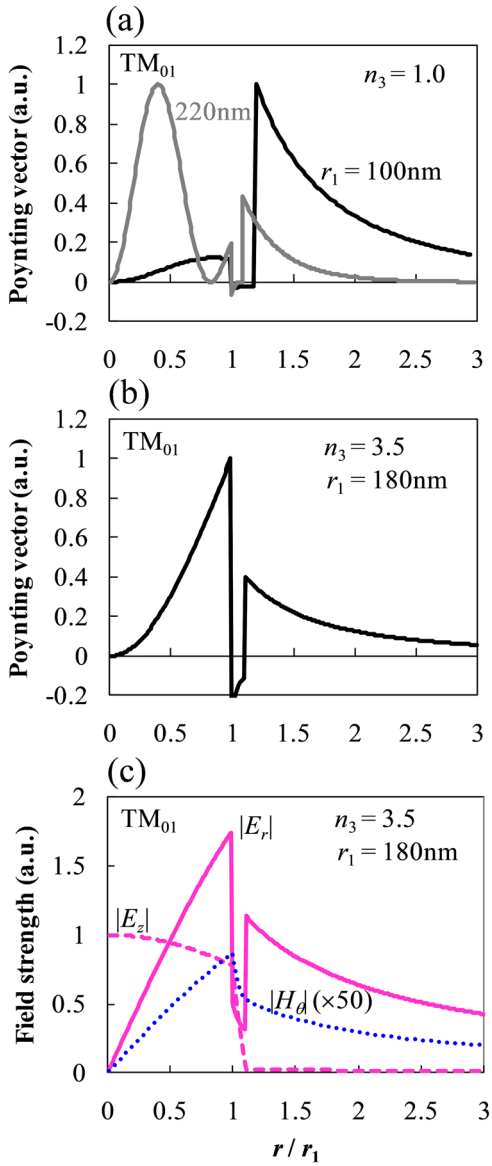

FIG. 5. (Color online) (a) Poynting vector in z direction vs r when $n_3 = 1$, $r_1 = 100$ and 220 nm, (b) Poynting vector and (c) field distributions when $n_3 = 3.5$, $r_1 = 180$ nm, all for theTM_{01} mode.

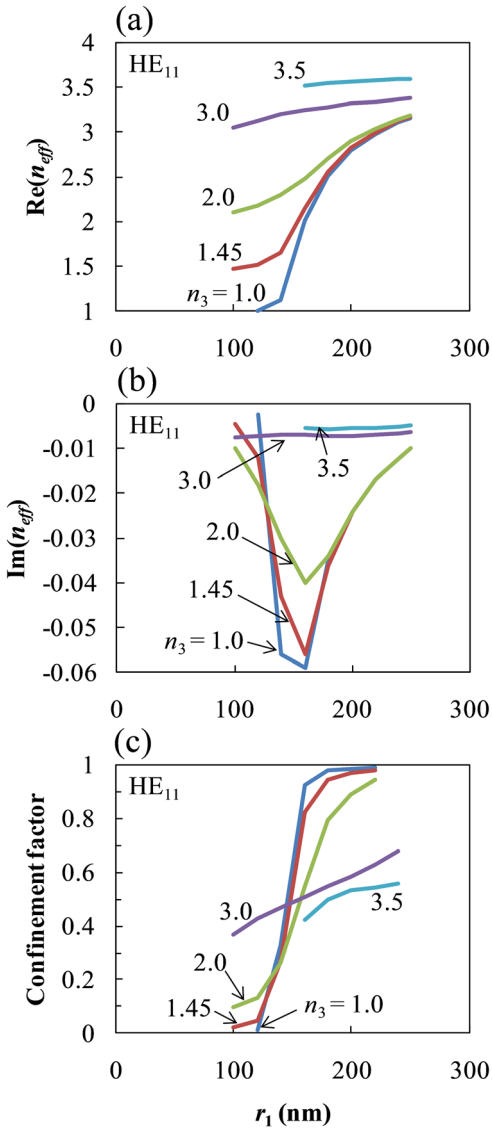

FIG. 6. (Color online) (a) Real and (b) imaginary parts of the calculated n_{eff} and (c) Poynting vector confinement factor, in relation to r_1 for the HE_{11} mode with $n_3 = 1$ to 3.5.

makes this mode useful for nanolaser applications as also seen in the TM_{01} mode.

IV. GAIN-ASSISTED PROPAGATIONS

We now examine gain-assisted propagation of the modified long-range SPP modes by including a positive imaginary value in n_1, which corresponds to the material gain. In Fig. 8(a), imaginary parts of calculated n_{eff} for the TM_{01} mode in relation to the imaginary part of n_1 are plotted for different n_3 with solid lines. The r_1 used for each n_3 is around the cutoff radius (i.e., $r_1 = 100$, 120, and 180 nm for $n_3 = 1.0$, 2.0, and 3.5, respectively). In order to verify our calculation, results calculated using the finite element method (FEM) from COMSOL are also plotted with the solid circles. In Fig. 8(a), some data are missing in the results from the matrix method where we could not find the solution. However, the data from the FEM well compensated the missing parts. The slight difference between the results from the matrix method and the FEM for $n_3 = 3.5$ will be from the effect of the computation space boundary in the FEM since the r_1 used is the largest. Indeed, the difference became larger when the space dimensions were made smaller. We observe that the tilts become larger for a larger n_3, which indicates the efficient amplification with a larger n_3 thanks to the larger mode confinement. Even for $n_3 = 1.0$, lossless propagation (i.e., $\mathrm{Im}(n_{eff}) > 0$) can be achieved with small material gain due to the small cold modal loss. However, since the modal gain cannot grow efficiently with increasing material gain, it will be difficult to compensate for the loss at the reflection in a laser resonator. The above discussion is also applicable to the HE_{11} mode.

We have shown efficient amplification of the long-range SPP modes using a high index outermost cladding. However, a larger optical power still resides in the outermost cladding for the TM_{01} mode since the confinement factor is about 0.3.

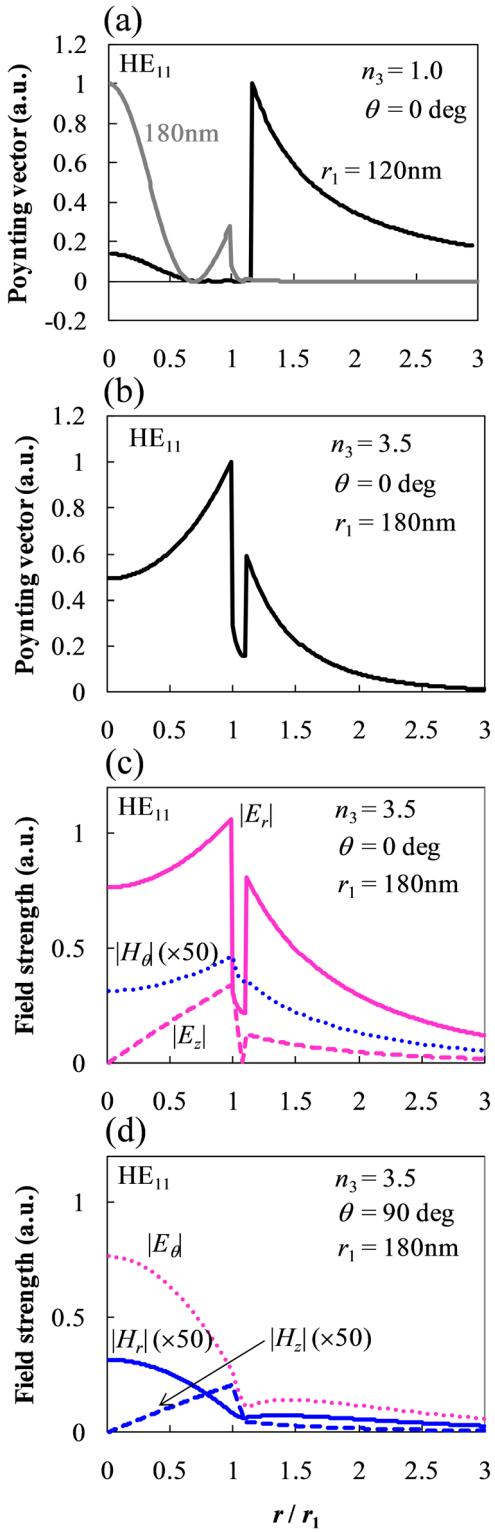

FIG. 7. (Color online) (a) Poynting vector in z direction at an azimuth of $\theta = 0$ deg vs r when $n_3 = 1$, $r_1 = 120$ and 180 nm, (b) Poynting vector at $\theta = 0$ deg, (c) and (d) field distributions at $\theta = 0$ and 90 deg when $n_3 = 3.5$, $r_1 = 180$ nm, all for the HE_{11} mode.

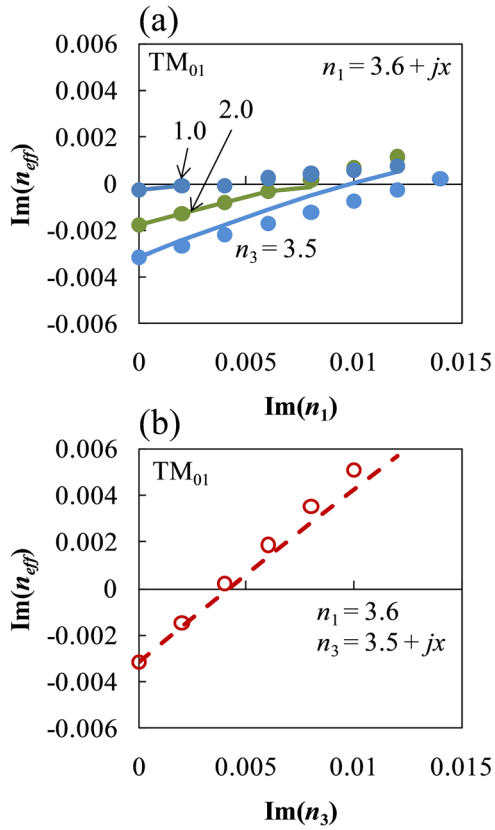

FIG. 8. (Color online) (a) Imaginary parts of calculated n_{eff} for the TM_{01} mode in relation to the imaginary part of n_1 are plotted for different n_3 with the solid lines (matrix method) and solid circles (FEM). The r_1 used for each n_3 is around the cutoff radius (i.e., $r_1 = 100$, 120, and 180 nm for $n_3 = 1.0$, 2.0, and 3.5, respectively). (b) The case with $n_1 = 3.6$, $\mathrm{Re}(n_3) = 3.5$ and different $\mathrm{Im}(n_3)$ is plotted by the dotted line and open circles.

In our structure, the refractive index of the outermost cladding is very high and the material may be a semiconductor with gain. Thus, it will be interesting to investigate a case with a real n_1 and a complex n_3. The case with $n_1 = 3.6$, $\mathrm{Re}(n_3) = 3.5$ and different $\mathrm{Im}(n_3)$ is plotted in Fig. 8(b) by the dotted line and open circles. We can see, as expected, that much more efficient amplification can be achieved with the gain in cladding. Such a structure could be fabricated by drilling a hole in a semiconductor gain material, depositing a thin insulator and a thin metal shell, and finally an amorphous semiconductor as a core material. Amorphous silicon is a candidate material for the core, which is a widely used material and whose refractive index could be well controlled by changing the deposition parameters.[15,16]

Finally, we compare the TM_{01} and HE_{11} modes in a specific structure with $n_3 = 3.5$ and $r_1 = 180$ nm. The TE_{01} mode does not exist in this structure since it is smaller than the cutoff radius. In other words, the long-range SPP mode of TM_{01} or HE_{11} is the first possible lasing mode for a nanolaser with this waveguide structure, depending on where the gain region is located. Figure 9(a) shows imaginary parts of calculated n_{eff} for the two modes in relation to the imaginary part of n_1 (core gain) or n_3 (clad gain). Figure 9(b) describes the power profiles of the TM_{01} and HE_{11} modes calculated by the FEM, which corresponds to Fig. 5(b) and Fig. 7(b) calculated by the matrix method. We observe that the HE_{11} mode is more efficiently gain-assisted than the TM_{01} mode for the core gain, while the TM_{01} mode with the clad gain is the most efficiently gain-assisted, just reflecting the modal confinement factors given in Fig. 4(c) and Fig. 6(c).

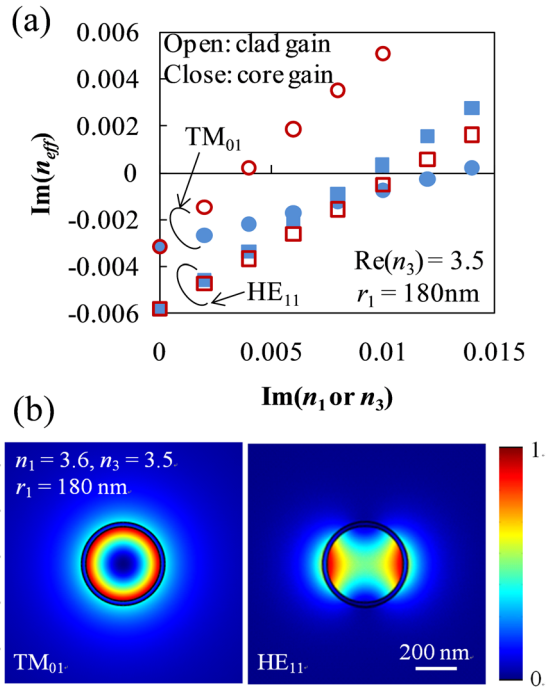

FIG. 9. (Color online) (a) Imaginary parts of calculated n_{eff} for the TM_{01} and HE_{11} modes in relation to the imaginary part of n_1 (core gain: $n_1 = 3.6 + jx$) or n_3 (clad gain: $n_3 = 3.5 + jx$) when $\mathrm{Re}(n_3) = 3.5$ and $r_1 = 180$ nm, (b) power profiles of the TM_{01} and HE_{11} modes calculated by the FEM for the same structure.

V. CONCLUSIONS

In conclusion, we have introduced a modification of long-range SPP modes supported by thin metal-coated dielectric cylinders for laser nanoresonators. We show that increasing the refractive index of the outermost dielectric cladding improves the poor mode overlap with the core semiconductor, but still keeps the mode low loss and well confined in a small radius of the cylinder. The high refractive index of the dielectric cladding offers another possibility of nanolaser structure whose gain region sits in the cladding, where the efficient modal gain can be achieved.

ACKNOWLEDGMENTS

Financial support from the Nakajima Foundation and the "R&D Promotion Scheme Funding International Joint Research" promoted by NICT are gratefully acknowledged. K.I. acknowledges helpful discussions with Dr. A. Mizrahi at UCSD. K.A.S. acknowledges support from the Invitation Fellowship Programs for Research in Japan by JSPS.

[1]M. T. Hill, Y.-S. Oei, B. Smalbrugge, Y. Zhu, T. de Vries, P. J. van Veldhoven, F. W. M. van Otten, T. J. Eijkemans, J. P. Turkiewicz, H. de Waardt, E. J. Geluk, S.-H. Kwon, Y.-H. Lee, R. Nötzel, and M. K. Smit, Nature Photon. **1**, 589 (2007).
[2]M. T. Hill, M. Marell, E. S. P. Leong, B. Smalbrugge, Y. Zhu, M. Sun, P. J. van Veldhoven, E. J. Geluk, F. Karouta, Y.-S. Oei, R. Nötzel, C.-Z. Ning, and M. K. Smit, Opt. Express **17**, 11107 (2009).
[3]M. P. Nezhad, A. Simic, O. Bondarenko, B. Slutsky, A. Mizrahi, L. Feng, V. Lomakin, and Y. Fainman, Nature Photon. **4**, 395 (2010).
[4]C.-Y. Lu, S.-W. Chang, S. L. Chuang, T. D. Germann, and D. Bimberg, Appl. Phys. Lett. **96**, 251101 (2010).
[5]V. Krishnamurthy and B. Klein, IEEE J. Quantum Electron. **44**, 67 (2008).
[6]D. Sarid, Phys. Rev. Lett. **47**, 1927 (1981).
[7]J. J. Burke, G. I. Stegeman, and T. Tamir, Phys. Rev. B **33**, 5186 (1986).
[8]I. De Leon and P. Berini, Nature Photon. **4**, 382 (2010).
[9]M. C. Gather, K. Meerholz, N. Danz, and K. Leosson, Nature Photon. **4**, 457 (2010).
[10]S. J. Al-Bader and M. Imtaar, IEEE J. Quantum Electron. **28**, 525 (1992).
[11]P. Yeh, A. Yariv, and E. Marom, J. Opt. Soc. Am. **68**, 1196 (1978).
[12]A. Mizrahi, V. Lomakin, B. A. Slutsky, M. P. Nezhad, L. Feng, and Y. Fainman, Opt. Lett. **33**, 1261 (2008).
[13]V. R. Almeida, Q. Xu, C. A. Barrios, and M. Lipson, Opt. Lett. **29**, 1209 (2004).
[14]R. F. Oulton, V. J. Sorger, D. A. Genov, D. F. P. Pile, and X. Zhang, Nature Photon. **2**, 496 (2008).
[15]K. Ikeda, Y. Shen, and Y. Fainman, Opt. Express **15**, 17761 (2007).
[16]Y. Shoji, T. Ogasawara, T. Kamei, Y. Sakakibara, S. Suda, K. Kintaka, H. Kawashima, M. Okano, T. Hasama, H. Ishikawa, and M. Mori, Opt. Express **18**, 5668 (2010).